Research Article | Vol. 28, No. 11 / 25 May 2020 / Optics Express 16511

Optics EXPRESS

Minimalist Mie coefficient model

ASO RAHIMZADEGAN,[1,4] RASOUL ALAEE,[2,5] CARSTEN ROCKSTUHL,[1,3] AND ROBERT W. BOYD[2]

[1] Institute of Theoretical Solid State Physics, Karlsruhe Institute of Technology, 76131 Karlsruhe, Germany
[2] Department of Physics, University of Ottawa, Ottawa, ON K1N 6N5, Canada
[3] Institute of Nanotechnology, Karlsruhe Institute of Technology, 76021 Karlsruhe, Germany
[4] aso.rahimzadegan@kit.edu
[5] rasoul.alaee@gmail.com

Abstract: When considering light scattering from a sphere, the ratios between the expansion coefficients of the scattered and the incident field in a spherical basis are known as the Mie coefficients. Generally, Mie coefficients depend on many degrees of freedom, including the dimensions and electromagnetic properties of the spherical object. However, for fundamental research, it is important to have easy expressions for all possible values of Mie coefficients within the existing physical constraints and which depend on the least number of degrees of freedom. While such expressions are known for spheres made from non-absorbing materials, we present here, for the first time to our knowledge, corresponding expressions for spheres made from absorbing materials. To illustrate the usefulness of these expressions, we investigate the upper bound for the absorption cross section of a trimer made from electric dipolar spheres. Given the results, we have designed a dipolar ITO trimer that offers a maximal absorption cross section. Our approach is not limited to dipolar terms, but indeed, as demonstrated in the manuscript, can be applied to higher order terms as well. Using our model, one can scan the entire accessible parameter space of spheres for specific functionalities in systems made from spherical scatterers.

1. Introduction

The solution for the scattering of light from a sphere was published by Gustav Mie more than a hundred years ago [1]. Although Ludwig Lorenz published the complete solution much earlier, the solution to the problem is widely attributed to Mie and is known as the Mie theory [2–8].

In Mie theory, the ratios between the scattered and the incident field coefficients in a spherical basis are expressed in terms of the Mie coefficients. Mie coefficients depend in an intricate manner on the spheres' radius and the involved material properties of both the sphere and the ambient (see our later Eq. (19)). The expressions become even more cumbersome when considering core-multishell or colloidal particles [9,10]. Moreover, electric and magnetic Mie coefficients of different multipolar orders can not be chosen independently. Each specific core-shell particle is characterized by a specific set of Mie coefficients. In the simplest case of a homogeneous sphere, it is just the radius and the permittivity of the sphere and the surrounding that unambiguously determines all the electric and magnetic Mie coefficients.

There are several algorithms and approximations for easier and more reliable calculation of Mie coefficients with the same level of complexity [11–14], but to enable a systematic analysis of the physically accessible optical properties from an individual or an aggregate of spherical objects, these explicit expressions are not that useful. They are too complicated, interdependent, and contain too many degrees of freedom. For fundamental research, it is of utmost importance to have easy expressions at hand with a minimal number of degrees of freedom that can capture all physically possible values of Mie coefficients independently. The precise geometrical and material properties of a sphere that offers these coefficients can be identified in a second step. But if these accessible coefficients depend on the least number of degrees of freedom, they would

#390331 https://doi.org/10.1364/OE.390331
Journal © 2020 Received 17 Feb 2020; revised 20 Apr 2020; accepted 20 Apr 2020; published 18 May 2020

Optics EXPRESS

allow for a systematic analysis of all observable effects using arrangements of spherical scatterers. Moreover, once the Mie coefficients of each sphere in an aggregate of spheres are known to offer a desired effect, afterward the structural detail of each sphere can be identified individually and it is not necessary to consider the entire ensemble. This is computationally much cheaper.

These desired simple expressions have been previously identified only for spheres made from non-absorbing materials [15–21]. Refer to the Appendix A for a discussion over the existing model. Corresponding expressions for spherical particles made from absorbing materials have not yet been reported and this is the center of focus of this paper. Here, while relying on the optical theorem, we derive generic expressions for any possible Mie coefficient a sphere made from absorbing materials may offer. These expressions depend on only two parameters (for each multipolar order and for each parity) that we call the *Mie angles*. Figure 1 shows the general idea of the article. We provide insights into the physical meaning of these Mie angles. At the example of the dipole coefficient, we show that the analytical space provided by the model is densely filled with electric and magnetic dipolar Mie coefficients of actual non-magnetic spheres. Moreover, based on our model, we will discuss scattering regimes such as critical coupling, over coupling, and weak coupling.

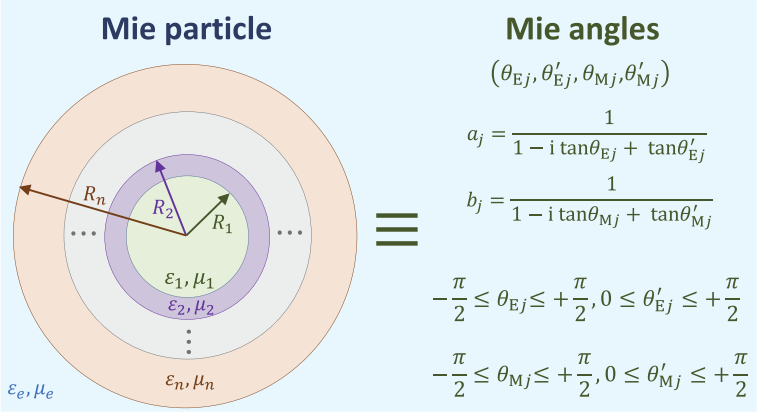

Fig. 1. *General idea of our proposal:* A minimal model to describe the electromagnetic response of spheres. The proposed *Mie angles* (right side of the figure) reduce the many degrees of freedom of an actual homogeneous or core-multishell sphere (left side of the figure) to only four Mie angles per multipolar order. These Mie angles express every possible Mie coefficient the scattering object may offer.

To demonstrate the applicability of our model, as a proof of principle, we investigate the upper bound for the absorption cross section of a trimer made from electric dipolar spheres using a multipolar analysis. Minimizing the degrees of freedom in our model allows to sweep through all possible combinations of the Mie angles and we can identify the Mie coefficients that are necessary to reach the maximum absorption cross section that is fundamentally possible. In a second step, we identify a homogeneous dipolar sphere, made from indium tin oxide (ITO), that offers these previously identified Mie coefficients. Hence, the trimer made from these ITO spheres reaches the upper bound for the absorption cross section. Clearly, the choice of material is not limited to ITO and another material could have been chosen as well. It is important to keep in mind that once a certain Mie coefficient combination is determined to satisfy the desired optical properties of an aggregate, the search for the desired parameters will be limited to that of the single object, rather than the entire aggregate. This is a reduction in the computation domain.

To illustrate that our model applicability is beyond a dipolar approximation, we have studied two more trimers; one made out of three electric quadrupolar spheres and one made out of three

Optics EXPRESS

electric dipolar - electric quadrupolar spheres. An electric dipolar - electric quadrupolar sphere is a particle with zero polarizabilities for all polarizability components except the electric dipole and electric quadrupole. We have identified the maximum absorption cross section of the trimers for a given illumination and have determined the required Mie angles to achieve those upper bounds.

Our model facilitates the systematic study of optical properties of systems constituting of single or multiple spheres made from absorbing or non-absorbing materials. The non-absorbing Mie model has already been used in identifying the fundamental limits of selected observable quantities, e.g. the optical force on individual particles [21]. Furthermore, it allowed designing metasurfaces for full phase coverage applications [22]. Moreover, it has been useful in systematic study of the generalized second Kerker condition [23]. Mie theory is one of the backbones of research in metamaterials and metasurfaces [24–34]. Introducing a general Mie model to include absorbing particles opens new ways in the optical design for thermal cooling [35,36], thermal emission [37–39], perfect absorption [40–43], non-local homogenization [44,45], metasurface holography [46–49], disordered photonics [50–52], optical manipulation [53–57], and many others.

2. Developing the model

The scattering, extinction, and absorption cross sections of an isotropic particle, i.e. a sphere, illuminated with a plane wave can be written in terms of its Mie coefficients as [4]:

$$C_{\text{sca}} = \frac{\lambda^2}{2\pi}\sum_{j=1}^{\infty}(2j+1)\left(|a_j|^2+|b_j|^2\right), \tag{1}$$

$$C_{\text{ext}} = \frac{\lambda^2}{2\pi}\sum_{j=1}^{\infty}(2j+1)\,\Re\left(a_j+b_j\right), \tag{2}$$

$$C_{\text{abs}} = \frac{\lambda^2}{2\pi}\sum_{j=1}^{\infty}(2j+1)\left[\Re\left(a_j+b_j\right)-\left(|a_j|^2+|b_j|^2\right)\right], \tag{3}$$

where λ is the illumination wavelength in the medium and a_j and b_j are the *electric and magnetic* Mie coefficients of the j's multipolar order, respectively.

Let us first consider the electric contribution. The contribution of a single electric Mie channel a_j to the total cross sections is:

$$C_{\text{sca,E}j} = (2j+1)\,\frac{\lambda^2}{2\pi}|a_j|^2, \tag{4}$$

$$C_{\text{ext,E}j} = (2j+1)\,\frac{\lambda^2}{2\pi}\Re\left(a_j\right), \tag{5}$$

$$C_{\text{abs,E}j} = (2j+1)\,\frac{\lambda^2}{2\pi}\left[\Re\left(a_j\right)-|a_j|^2\right]. \tag{6}$$

Since the channels do not mix, the optical theorem requires that $C_{\text{ext,E}j} = C_{\text{abs,E}j} + C_{\text{sca,E}j}$.

2.1. Mie angles for non-absorbing particles

Assuming that the particle is made from a non-absorbing material, i.e. $C_{\text{abs,E}j} = 0$, based on the optical theorem we require that:

$$\Re\left(a_j\right) = |a_j|^2. \tag{7}$$

Writing a_j in an exponential form as $a_j = |a_j|\exp\left(\mathrm{i}\theta_{\text{E}j}\right)$, with $\theta_{\text{E}j} = \arg\left(a_j\right)$ as what we call the Mie angle, and replacing it in Eq. (7), we can conclude that $\cos\left(\theta_{\text{E}j}\right) = |a_j|$. Therefore, we can

Optics EXPRESS

write [21]:

$$a_j = \cos\left(\theta_{\mathrm{E}j}\right) \exp\left(\mathrm{i}\theta_{\mathrm{E}j}\right), \tag{8}$$

where $-\pi/2 \leqslant \theta_{\mathrm{E}j} \leqslant +\pi/2$ directly follows. The expression captures any possible Mie coefficient that agrees with the optical theorem. Sweeping through the full angular range, the possible Mie coefficients trace out a circle in the complex plane with a radius of 0.5 that is centered at $(0\mathrm{i}, 0.5)$. An illustration of that functional dependence of the Mie coefficient is shown in Fig. 2(a) as the red line. The Mie coefficient at the resonance of the particle attains its maximum value, which is 1. The corresponding Mie angle for a sphere made from a non-absorbing material is $\theta_{\mathrm{E}j} = 0$. According to Eqs. (4)–(6), the scattering/extinction cross section maximizes to $(2j+1)\lambda^2/(2\pi)$, , i.e. in the overcoupling regime [21,58].

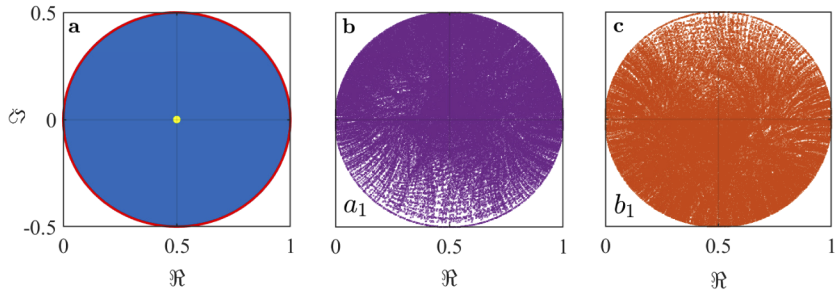

Fig. 2. *Potential and actual Mie coefficient values:* a) Here, all physically possible values for Mie coefficients in the complex plane based on the optical theorem (using Eq. (10)) are illustrated. For a non-absorbing sphere, the physically possible values are on the red circle. For an absorbing sphere, the physically possible values are within the blue area. The yellow dot in the center shows the point of critical coupling. b) Electric and c) magnetic dipolar Mie coefficient of homogeneous spheres embedded in the free space with discrete radius $R_s \in [0.45 : 0.005 : 0.75]\lambda$, discrete permittivity $\Re(\epsilon_r) \in [0 : 0.5 : 20]$, $\Im(\epsilon_r) \in [0 : 0.025 : 1]$ and permeability $\mu_r = 1$ using Eq. (19). Each marker point shows an individual realization. The purpose is to show that indeed with homogeneous spheres in this parameter regime, every physically possible electric/magnetic dipolar Mie coefficient can be achieved. The remaining empty spaces in these figures remain because of a finite sampling of our data plots, we plot here only a discrete number of samples. The entire disk will be covered if finer data points are plotted.

2.2. Mie angles for absorbing particles

For a sphere made from absorbing materials, we simply require that absorption shall be finite. Passivity, as we assume here, implies that the absorption cross section is positive. Based on the optical theorem the extinction cross section is required to be larger or equal to the scattering cross section. With that as a starting point and by a similar line of arguments, we obtain

$$C_{\mathrm{ext,E}j} \geq C_{\mathrm{sca,E}j} \Longrightarrow \Re\left(a_j\right) \geq |a_j|^2 \Longrightarrow \cos\theta_{\mathrm{E}j} \geq |a_j|. \tag{9}$$

The derived inequality on the right covers the entire space enclosed by the red circle in Fig. 2. This space is highlighted with a blue color. Therefore, as a general rule, the Mie coefficient of a passive isotropic particle, be it absorbing or non-absorbing, must be on top of or inside the red circle in Fig. 2(a), i.e. within the blue area shown in this figure. It can be immediately inferred from this limit that the real part of any Mie coefficient is always positive. Hence, a combination of the Mie coefficient where $a_j = -b_j$, which was called in literature as anti-dual [59], in contrast to a dual combination where $a_j = b_j$, is not possible for passive particles.

Optics EXPRESS

We aim to find a model that respects the physical limitations, that covers the entire area previously identified as accessible with the least number of parameters, and which simultaneously allows a physical interpretation. We suggest here to model the general form of a Mie coefficient as:

$$a_j = \frac{1}{\frac{1}{\cos\theta_{\mathrm{E}j}\exp \mathrm{i}\theta_{\mathrm{E}j}} + \tan\theta'_{\mathrm{E}j}} = \frac{1}{1 - \mathrm{i}\tan\theta_{\mathrm{E}j} + \tan\theta'_{\mathrm{E}j}}, \tag{10}$$

where $-\frac{\pi}{2} \leqslant \theta_{\mathrm{E}j} \leqslant +\frac{\pi}{2}$ and $0 \leqslant \theta'_{\mathrm{E}j} \leqslant +\frac{\pi}{2}$ are named the *detuning and absorption Mie angles*, respectively. The reason for this naming will be justified later in the manuscript when discussing the physical meaning of the Mie angles. Equation (10) can also be derived from the actual formula for the Mie coefficient of a homogeneous non-magnetic sphere (shown in the Appendix B) and also from the Lorentzian polarizability model. Equation (10) is the main contribution of this paper. The expression is valid for any isotropic particle, homogeneous or core-multishell spheres.

To see if the Mie coefficients of actual spheres cover the possible space, we swept through the radius R_s and complex permittivity of a non-magnetic sphere and calculated the dipolar Mie coefficients (using Eq. (19)). The results are shown in Figs. 2(b) and (c). As can be seen, with realistic parameters the entire complex plane is filled. It shows that our model can be reliably used in analytic studies. Of course, the possible space is not homogeneously filled and an inhomogeneous density of points is observed. Similar results can be obtained for higher Mie coefficient orders and our model is valid for dipoles, quadrupoles and so forth.

Note that due to duality-symmetry [6], fixing the permittivity and sweeping through the permeability will result in identical outcomes. Furthermore, since the disk is already filled with the current parameters, we have not simultaneously changed the permeability and permittivity.

Moreover, note that changing the actual properties of an object changes not only the dipolar Mie coefficients but also all higher-order coefficients simultaneously. This interdependence is a troubling drawback in systematic design. Using the Mie angles instead, allows us to change all coefficients independently. At the same time, we can be sure that the calculated Mie coefficients are realistic and with sufficient efforts, an object can in principle be identified that offers these coefficients. This method is especially useful for smaller spheres that require a fewer number of multipoles to capture their response, i.e. up to quadrupolar order. For completeness, it is worth mentioning that for homogeneous spheres there are recurrence equations such that octopolar Mie coefficients can be derived from dipolar and quadrupolar Mie coefficients [60].

The optical cross sections for the previously considered isolated electric multipolar contribution, Eqs. (4)–(6), expressed in terms of the Mie angles are:

$$C_{\mathrm{sca,E}j} = (2j+1)\,\frac{\lambda^2}{2\pi}\,\frac{1}{\left(1+\tan\theta'_{\mathrm{E}j}\right)^2 + \tan^2\theta_{\mathrm{E}j}}, \tag{11}$$

$$C_{\mathrm{ext,E}j} = (2j+1)\,\frac{\lambda^2}{2\pi}\,\frac{1+\tan\theta'_{\mathrm{E}j}}{\left(1+\tan\theta'_{\mathrm{E}j}\right)^2 + \tan^2\theta_{\mathrm{E}j}}, \tag{12}$$

$$C_{\mathrm{abs,E}j} = (2j+1)\,\frac{\lambda^2}{2\pi}\,\frac{\tan\theta'_{\mathrm{E}j}}{\left(1+\tan\theta'_{\mathrm{E}j}\right)^2 + \tan^2\theta_{\mathrm{E}j}}. \tag{13}$$

Note that the optical cross sections for the magnetic contributions are similar to those shown in Eqs. (11)–(13). It simply requires that we replace $\theta_{\mathrm{E}j}$, and $\theta'_{\mathrm{E}j}$ with $\theta_{\mathrm{M}j}$, and $\theta'_{\mathrm{M}j}$. The results of the normalized optical cross sections as a function of the Mie angles for an individual electric multipolar contribution are shown in Fig. 3. The normalization factors $(2j+1)\lambda^2/2\pi$,

Optics EXPRESS

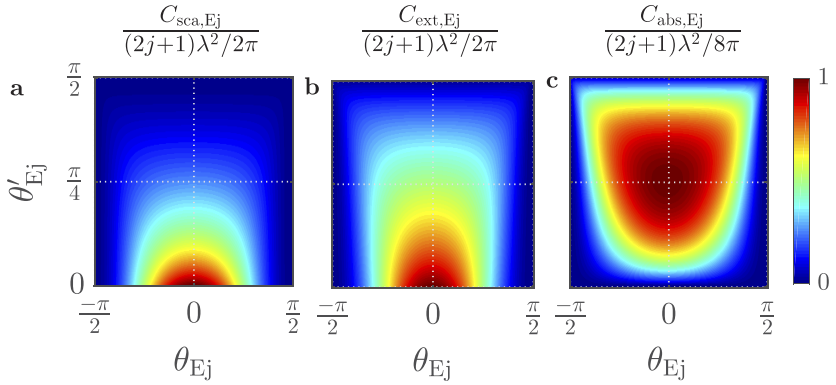

Fig. 3. *Optical cross sections as a function of the Mie angles:* The normalized a) scattering, b) extinction, and c) absorption cross sections as a function of the Mie angles (i.e. $\theta_{\mathrm{E}j}$ and $\theta'_{\mathrm{E}j}$) using Eqs. (11)–(13).

$(2j+1)\lambda^2/2\pi$, and $(2j+1)\lambda^2/8\pi$ are the maximum scattering, extinction, and absorption cross section of a single resonance with multipolar order of j, respectively [21,58].

As expected, the scattering cross section in Fig. 3(a) is maximum when there is no absorption (i.e. $\theta'_{\mathrm{E}j}=0$) and the detuning from the resonance is zero (i.e. $\theta_{\mathrm{E}j}=0$). The same holds for the extinction cross section. In the absorption cross section, the maximum, i.e. the critical coupling, occurs when the detuning is zero ($\theta_{\mathrm{E}j}=0$) and the absorption angle is $\pi/4$ ($\theta'_{\mathrm{E}j}=\pi/4$).

3. Physical interpretation of Mie angles

To ease the physical interpretations of the Mie angles, we use the Lorentzian dispersion profile for the polarizability of an isotropic particle and study how the model parameters fit the physical properties of a resonance. The dynamic polarizability of a dipolar resonance can be modeled with a Lorentzian dispersion as [61]:

$$\alpha = -\frac{6\pi}{k_0^3}\frac{\gamma_r/2}{\delta+(\gamma_{\mathrm{nr}}+\gamma_{\mathrm{r}})\mathrm{i}/2}, \tag{14}$$

where, $\delta=\omega-\omega_0$, with $|\delta|<<\omega_0$ is the frequency detuning between the excitation and the resonance frequency ω_0, k_0 is the wave number at the resonance, and γ_r and γ_{nr} are the radiative and non-radiative losses of the resonance. Exploiting the relation between the Mie coefficient and the polarizability, i.e. $a_1=\frac{k^3}{6\pi\mathrm{i}}\alpha$ for the electric dipole Mie coefficient, we get:

$$\frac{1}{a_1}=\frac{-2\delta}{\gamma_{\mathrm{r}}}\mathrm{i}+\frac{\gamma_{\mathrm{nr}}}{\gamma_{\mathrm{r}}}+1. \tag{15}$$

A direct comparison of this equation with Eq. (10) results in:

$$\tan\theta_{\mathrm{E1}}=\frac{2\delta}{\gamma_{\mathrm{r}}},\tan\theta'_{\mathrm{E1}}=\frac{\gamma_{\mathrm{nr}}}{\gamma_{\mathrm{r}}}. \tag{16}$$

Therefore, for any resonance, one can conclude that $\theta_{\mathrm{E}j}$ represents detuning and $\theta'_{\mathrm{E}j}$ represents Ohmic losses, i.e. absorption. This is under the assumption that the polarizability corresponding to the Mie resonance is Lorentzian. For instance, a high refractive index or metallic spheres can have Lorentzian polarizability [40,62]. Note that Eq. (16) is very similar to the *electric loss*

Optics EXPRESS

tangent defined as the ratio between the imaginary part of the permittivity to its real part for absorbing bulk material. Using duality symmetry, one can show that the magnetic Mie coefficient can be written similar to Eq. (15). Therefore, we can also define magnetic detuning, absorption angles, and *magnetic loss tangent*. The magnetic loss tangent is the ratio between the imaginary part of the permeability to its real part.

4. Mie angles of spheres

In this section, we explore the functional dependence of the Mie angles for actual spheres. Figure 4 shows the dipolar electric and magnetic Mie angles for a homogeneous non-absorbing sphere depending on the permittivity of the sphere's material and depending on the ratio of the sphere's radius to the free space wavelength. The surrounding medium is assumed to be a vacuum. In Fig. 4, the Mie angles show the recurrence of resonances and the expected pattern change that the size of the sphere enforces. The bigger the sphere, the more resonances are observed by changing the permittivity. A resonance is identified as the point in the parameter space where the Mie angles are zero. Electric and magnetic resonance are not occurring at

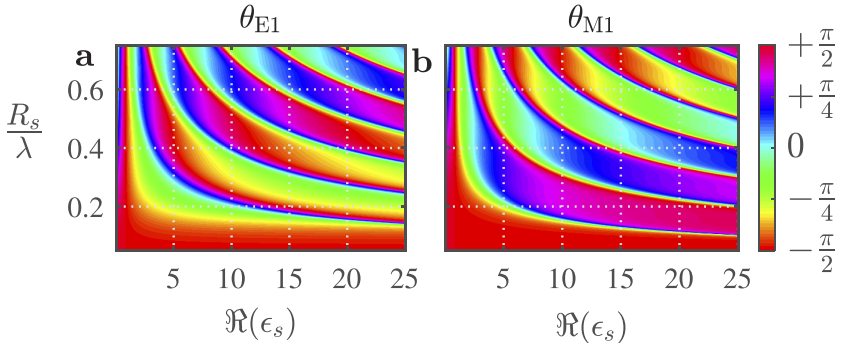

Fig. 4. *Non-absorbing particle:* The dipolar electric (a) and magnetic (b) Mie angles (i.e. θ_{E1} and θ_{M1}) for a non-absorbing and non-magnetic sphere embedded in the free space as a function of sphere radius R_s and $\Re(\epsilon_r)$. Derived from the calculated Mie coefficients using Eq. (19) and Eq. (10).

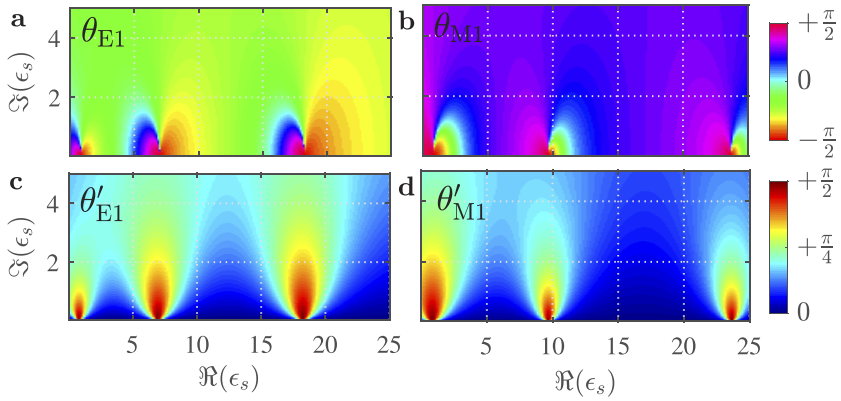

Fig. 5. *Absorbing particle:* The dipolar electric and magnetic Mie angles (i.e. θ_{E1} and θ_{M1}) for an absorbing sphere with a normalized radius of $R_s/\lambda = 0.25$ as a function of the real and imaginary part of the sphere's material. Derived from the calculated Mie coefficients using Eqs. (19) and Eq. (10).

Optics EXPRESS

the same parameter point, a clear indication that making dual-symmetric spheres with strong scattering response is challenging. Moreover, for small spheres with a low refractive index, satisfying the duality symmetry is easier [63]. However, as perceived from the figure, in the low-refractive-index regime the Mie angles are far away from the resonance (scattering angle of 0 as shown in the cyan color) and hence the scattering is weak.

Figure 5 shows the dipolar electric and magnetic Mie angles for a homogeneous absorbing sphere as a function of the real and imaginary part of the permittivity of the sphere's material for a fixed size. For a non-absorbing sphere, i.e. $\Im(\epsilon_s) = 0$, for the permittivity range considered in the figure, three resonances are observed. By increasing the imaginary part of the permittivity, the Mie angles, as seen in the figure, gradually fade away. Note that by comparing Fig. 3 and Fig. 5, it is clear that a large imaginary part for the permittivity does not necessarily lead to a large absorption.

5. Trimers with maximum absorption

Having defined the Mie angles and how they affect the properties of isolated spheres, we give an example for a specific design challenge to demonstrate the applicability of our model. We wish to answer the question of what is the maximum absorption cross section of three spherical multipolar particles arranged at the corners of an equilateral trimer for a predefined illumination direction and polarization. Without a simple model, one might have to simulate all possible spherical (homogeneous, core-multishell, or colloidal) particles with different radii while changing their material properties. However, by using our model, one can easily address such question quasi-analytically. Here, to avoid complications, we limit our analysis to only three scenarios: a trimer made out of three electric dipoles, a trimer made out of three electric quadrupoles, and a trimer made out of three electric dipoles and quadrupoles. Obviously, the analysis can be extended to include many more multipoles to address the problem in a general fashion. However, here, we want to stay within the scope of the paper and focus on the applicability of the model. Note that for an illuminating wave-vector perpendicular to the surface of the triangle made by connecting the coordinates of the trimer particles, due to symmetry reasons, the optical cross sections are independent to the direction of the linear polarization [64].

5.1. Trimer made of out of three electric dipoles

For a trimer made out of three electric dipoles, if the particles are very distanced from one another, the coupling is negligible and the maximum cross section would be $3 \times C^{\max}_{\text{abs,E1}}$. This is three times larger than the maximum absorption cross section of an isolated electric dipolar particle, i.e. $C^{\max}_{\text{abs,E1}} = 3\lambda^2/(8\pi)$. However, if the particles are brought closer, their coupling changes the maximum possible absorption cross section. The question is what is the maximum possible absorption cross section of the electric dipolar trimer and which properties the spheres shall have in order to reach this maximum. Here, we identify as a first step the Mie angles that provide the maximum absorption cross section for a given side length of the equilateral trimer. A global maximum is identified by sweeping through the side length d. Once the optimal Mie angles are identified, we design actual particles that offer the required Mie angles.

We consider a trimer with a fixed side length d that at the corners identical isotropic electric dipolar spheres are placed. Their properties are expressed with the Mie model in Eq. (10). By sweeping through the detuning and the absorption Mie angle, the maximum absorption of the trimer normalized to $3 \times 3\lambda^2/(8\pi)$ for a fixed side length can be identified. Actual calculations are based on a multipolar analysis method [65–69]. In the multipolar analysis, the incident and scattered fields are projected onto vector spherical harmonics. The vectors containing their amplitude coefficients are connected via the T-matrix. In our case, as we are dealing with spherical particles, the T-matrix of a single scatterer is diagonal and the entries correspond to the Mie coefficients. For a discussion over the connection between the scattering matrix and the

Optics EXPRESS

T-matrix, refer to Appendix C. For the calculation of the absorption cross section, we have used a local-coordinate T-matrix method with multipolar order of 2, however, we have verified the results with a global-coordinate T-matrix method of multipolar order of 20. In local-coordinate system, we define all the coefficients in the local-coordinate system of each particle, whereas in the global T-matrix method, all the coefficients are computed with respect to a global reference point, i.e. here in the center of the trimers. The large multipolar order of 20 is required for converging results for large distances.

Representative results for a normalized distance of $d/\lambda = 0.5$ are shown in Fig. 6(a). For each distance d, there is a maximum absorption cross section. Figure 6(b) shows the maximum absorption cross section for any given distance d. The maximum possible absorption cross section of the trimer occurs at a distance of 0.725λ and it amounts to $1.52 \times 3 \times 3\lambda^2/(8\pi)$. This maximum theoretical limit occurs for the Mie angles of $\theta_{\mathrm{E1}} = 4^o$, $\theta'_{\mathrm{E}j} = 34.5^o$ that translate to specific Mie coefficients.

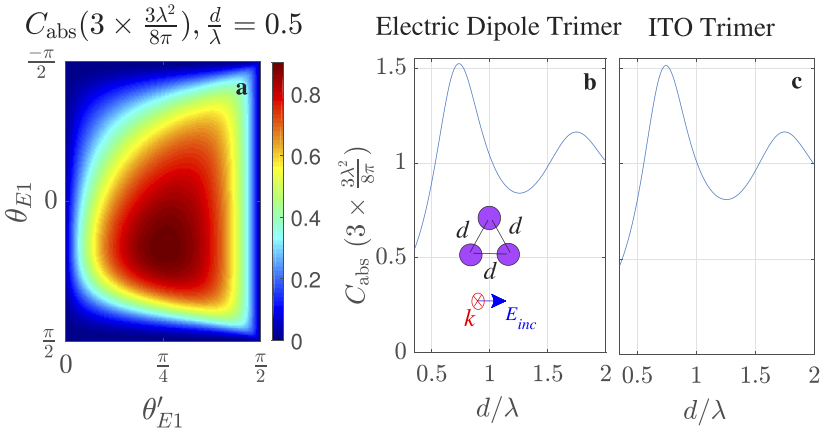

Fig. 6. *Maximum absorption cross section of a trimer:* a) The full map of the normalized absorption cross section of an equilateral trimer made from isotropic electric dipoles with a side length of $d = 0.5\lambda$ as a function of the Mie angles of the individual particle. The polarization and direction of the excitation are shown in the inset of part (b). b) The maximum absorption cross section of the trimer for any given distance. The global maximal absorption cross section occurs at a distance of $d = 0.725\lambda$ and the required Mie angles are: $\theta_{\mathrm{E1}} = 4^o$, $\theta'_{\mathrm{E1}} = 34.5^o$ (i.e. $a_1 = 0.59 + 0.02\mathrm{i}$). The inset figure shows the trimer with the assumed plane wave excitation polarization. c) The maximal absorption cross section for an optimized ITO trimer at a wavelength of λ =1740 nm designed based on the theoretical results derived from Fig. 6(b). The radius of the ITO spheres in the trimer is 179 nm.

Once we know the necessary Mie coefficients, we can identify actual spheres from real materials that offer these coefficients. Here, we consider spheres made from ITO. The permittivity of ITO is expressed as $\epsilon = \epsilon_\infty - \frac{\omega_p^2}{\omega(\omega+i\gamma)}$, where $\omega_p = 2\pi \times 4.24 \times 10^{14}$ rad/s, $\epsilon_\infty = 2.97$, $\gamma = 1.27 \times 10^{14}$ Hz [70]. By tuning the radius and wavelength of operation, we find that at a wavelength of 1740 nm an ITO sphere with a radius of 179 nm offers the required Mie coefficients. The absorption cross section of an equilateral triangle of such spheres as a function of the trimer side length is shown in Fig. 6(c). At a distance of $0.75\lambda = 1305$ nm, a maximum absorption cross section of $1.51 \times 3 \times 3\lambda^2/(8\pi)$ is reproduced as predicted by the theory.

To briefly summarize the methodology, for any given optical function that depend on the properties of wavelength-scale spherical constituents, we sweep through all possible Mie-angles and calculate the optical function with the computational tool we have at hand. Then, at the secondary step, we search for the particle or particles that satisfy the required Mie coefficients.

Optics EXPRESS

5.2. Trimers with beyond dipolar constituents

To show the applicability of our method beyond dipolar approximation, we also identify the maximum absorption cross section of a trimer made out of electric quadrupolar and electric dipolar- electric quadrupolar spheres illuminated with a plane wave with a polarization along the side of the equilateral triangle of the structure, the same as in Fig. 6. The procedure is similar to the previous section. We sweep through all possible Mie coefficients of the dipole and/or quadrupoles. Then, we determine the maximum cross section for each distance. The results are shown in Fig. 7(a). In Figs. 7(b) and (c) we have shown the required Mie angles to maximize the absorption cross section for each distance. An interesting finding is that the required angles in a trimer made out of electric dipolar-quadrupolar spheres is the same as the required angles for a trimer made out of electric dipoles and a trimer made out of electric quadrupoles. Clearly, adding more multipoles to our design, increases the computational burden. That is why our method is limited to small particles that a few multipolar orders are adequate to describe the response of the particle.

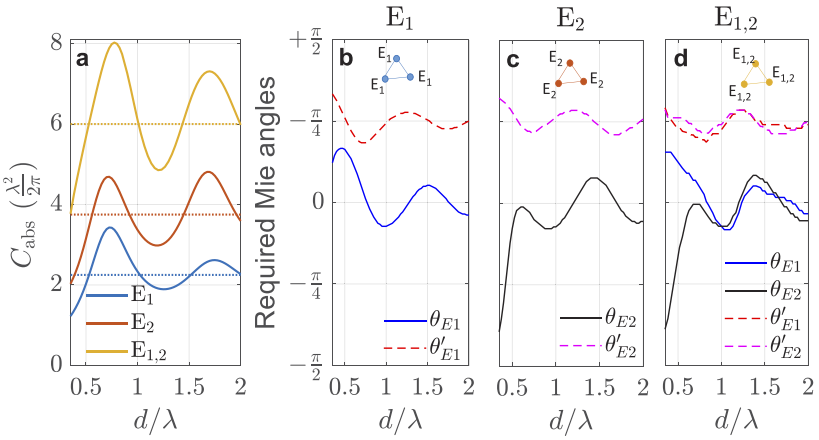

Fig. 7. *Maximum possible absorption cross section of three multipolar trimers:* a) The maximum absorption cross section of three different equilateral trimers made from isotropic electric dipoles, shown with legend E_1, isotropic electric quadrupoles, shown with legend E_2, and isotropic electric dipoles and quadrupoles, shown with the legend $E_{1,2}$ for any given distance. The plane wave excitation polarization is the same as in Fig. 6. The dotted lines of the same color show the maximum theoretical absorption cross section of the trimer, if no coupling is considered, i.e. at a distance of infinity. For E_1: $3\times\frac{3}{4}\times\frac{\lambda^2}{2\pi}$. For E_2: $3\times\frac{5}{4}\times\frac{\lambda^2}{2\pi}$. For $E_{1,2}$: $3\times(\frac{3}{4}+\frac{5}{4})\times\frac{\lambda^2}{2\pi}$. b) The required Mie angles to maximize the absorption cross section of the trimer made out of three electric dipoles, c) three electric quadrupole, and, d) three electric dipole - electric quadrupoles. Note that, whenever not mentioned, the other multipoles are assumed to be zero.

6. Conclusions

In conclusion, based on the optical theorem, we have proposed a general model to express any possible Mie coefficient of an isotropic sphere made from absorbing or non-absorbing materials. The corresponding Mie angles defined in the model are associated with the physical properties of the scatterer and hence are called the detuning angle and the absorption angle. The lower degree of freedom and the decoupling of the proposed parameters in the model allow for the systematic search for specific functionalities in absorbing and non-absorbing systems. In particular, all Mie coefficients that are admissible can be independently tuned without forcing the particle to

Optics EXPRESS

attain a specific geometry. Once the optimal Mie coefficients, in terms of the Mie angles for all multipolar orders, are identified to offer a desired functionality for the system, in a secondary step, actual individual spherical (homogeneous, core-multishell, or colloidal) particles can be designed that offer these desired Mie coefficients. The reduction of computational complexity in designing a single particle rather than an aggregate allows for faster computations. The design process of the individual particle might involve different optimization methods. For instance, we have been able to calculate the theoretical upper limit for the absorption cross section of an electric dipolar, electric quadrupolar and electric dipolar-quadrupolar trimer and have proposed actual dipolar ITO-spheres, based on the insights, that reach the upper bound. For the design of the individual spheres based on the derived Mie angles, we have used sweep simulations on homogeneous ITO spheres. This has been a fortunate example where actual homogeneous spheres could be identified that offer these optimal conditions for the simple scenario we have defined initially. For a general and more complicated scenarios, core-multishell or colloidal spheres might have been required to offer desired properties. There, the design process might require more complicated optimization methods and neural networks [71]. Our approach is valid for isotropic particles, but the insights can be extended to more general types of particles.

Appendix A: Mie angles vs. phase shifts

In Ref. [15] an expression similar to our model for the Mie coefficients of non-absorbing spheres is used, in which the Mie coefficients are represented by:

$$\begin{aligned} a_n &= \mathrm{i}\sin\alpha_n \exp\left(-\mathrm{i}\alpha_n\right), \\ b_n &= \mathrm{i}\sin\beta_n \exp\left(-\mathrm{i}\beta_n\right), \end{aligned} \tag{17}$$

where α_n and β_n are called the phase shifts or phase angles. The relation between the phase-shift and the Mie angles are as follows:

$$\begin{aligned} \alpha_n &= \frac{\pi}{2} - \theta_{\mathrm{E}j}, \\ \beta_n &= \frac{\pi}{2} - \theta_{\mathrm{M}j}, \end{aligned} \tag{18}$$

Appendix B: Deriving the Mie model

The Mie coefficients for a homogeneous sphere are defined as [2,3,6]:

$$\begin{aligned} a_n &= \frac{\mu_e \eta^2 j_n(\eta x)\left[x j_n(x)\right]' - \mu_s j_n(x)\left[\eta x j_n(\eta x)\right]'}{\mu_e \eta^2 j_n(\eta x)\left[x h_n^{(1)}(x)\right]' - \mu_s h_n^{(1)}(x)\left[\eta x j_n(\eta x)\right]'}, \\ b_n &= \frac{\mu_s j_n(\eta x)\left[x j_n(x)\right]' - \mu_e j_n(x)\left[\eta x j_n(\eta x)\right]'}{\mu_s j_n(\eta x)\left[x h_n^{(1)}(x)\right]' - \mu_e h_n^{(1)}(x)\left[\eta x j_n(\eta x)\right]'}, \end{aligned} \tag{19}$$

where subscript e and s denote the properties of the embedding and the sphere respectively. j and h denote the Bessel and Hankel functions respectively. The primes are derivatives with respect to the argument. The parameters x and η are defined as:

$$x = \frac{\omega}{c}\sqrt{\epsilon_e(\omega)\,\mu_e(\omega)}R_s, \quad \eta = \sqrt{\frac{\epsilon_s(\omega)\,\mu_s(\omega)}{\epsilon_e(\omega)\,\mu_e(\omega)}}, \tag{20}$$

where R_s is the radius of the sphere.

Optics EXPRESS

For an equal permeability of embedding and the sphere (i.e. $\mu_e = \mu_s$), the Mie coefficients can be reformulated as [16,17]:

$$a_j = \frac{P_j^e}{P_j^e + \mathrm{iQ_j^e}}, \; b_j = \frac{P_j^m}{P_j^m + \mathrm{iQ_j^m}}, \tag{21}$$

where P_j, Q_j are functions of Ricatti-Bessel functions. For a real refractive index, P_j, Q_j are real. However, for a general refractive index one can re-write:

$$\frac{1}{a_j} = 1 + \mathrm{i}\frac{\mathrm{Q_j^e}}{P_j^e} = 1 + \mathrm{i}\Re\left(\frac{\mathrm{Q_j^e}}{P_j^e}\right) - \Im\left(\frac{\mathrm{Q_j^e}}{P_j^e}\right). \tag{22}$$

Without lose of generality, we can write the real and imaginary parts as tangent of angles as follows:

$$\Re\left(\frac{\mathrm{Q_j^e}}{P_j^e}\right) = -\tan\theta_{\mathrm{E}j}, \;\; \Im\left(\frac{\mathrm{Q_j^e}}{P_j^e}\right) = -\tan\theta'_{\mathrm{E}j}. \tag{23}$$

While there is no limitations on the real part, for absorbing particles, $\Im\left(\frac{\mathrm{Q_j^e}}{P_j^e}\right)$ should be negative and therefore: $-\frac{\pi}{2} \leqslant \theta_{\mathrm{E}j} \leqslant +\frac{\pi}{2}$ and $0 \leqslant \theta'_{\mathrm{E}j} \leqslant +\frac{\pi}{2}$, which is what we have in Eq. (10).

Appendix C: T-matrix and the scattering matrix

The Mie coefficients that we model are the entries on the diagonal of the T-matrix for a sphere. The T-matrix in general describes how a specific vector spherical harmonic (VSH) used to expand the incident field is scattered by an object into a specific VSH used to expand the scattered field [65]. For an arbitrary object with no particular symmetry, any incident VSH can scatter into any scattered VSH. For a sphere, where the rotational symmetry excludes any cross-coupling between VSH that do not share the same quantum numbers in their expansion, no such cross-coupling can happen and the T-matrix is diagonal.

Once the T-matrix $\mathbf{T}$ is known, the relationship to the scattering matrix $\mathbf{S}$ can be written as $\mathbf{S} = \mathbf{I} + 2\mathbf{T}$, with $\mathbf{I}$ being the identity matrix [72]. The difference in the physical meaning between T- and scattering matrix is well known; While the T-matrix maps the incident to the scattered field, the scattering matrix maps the incoming to the outgoing field. The scattered field contains only an outgoing component, while the incident field contains both the incoming and the outgoing components, which causes the difference in the expressions.

Funding

Deutsche Forschungsgemeinschaft (278747906, 390761711); Karlsruhe School of Optics and Photonics; Alexander von Humboldt-Stiftung (Feodor Lynen Fellowship); Natural Sciences and Engineering Research Council of Canada; Canada Research Chairs; Canada First Research Excellence Fund.

Acknowledgments

We acknowledge support by the German Research Foundation in the priority program SPP 1839 Tailored Disorder (RO 3640/7-2 under project number 278747906) and from the Excellence Cluster 3D Matter Made to Order (EXC 2082/1 under project number - 390761711). A. Rahimzadegan acknowledges support from the Karlsruhe School of Optics and Photonics (KSOP). R.A. acknowledges the support of the Alexander von Humboldt Foundation through the Feodor Lynen Fellowship. R.W.B. acknowledges support through the Natural Sciences and Engineering Research Council of Canada, the Canada Research Chairs program, and the Canada First Research Excellence Fund.

Optics EXPRESS

Disclosures

The authors declare no conflicts of interest.

References

1. G. Mie, "Beiträge zur Optik trüber Medien, speziell kolloidaler Metallösungen," Ann. Phys. **330**(3), 377–445 (1908).
2. C. F. Bohren and D. R. Huffman, *Absorption and Scattering of Light by Small Particles* (John Wiley & Sons, 2008).
3. J. A. Stratton, *Electromagnetic theory* (John Wiley & Sons, 2007).
4. M. Born and E. Wolf, *Principles of Optics: Electromagnetic Theory of Propagation, Interference and Diffraction of Light* (Elsevier, 2013).
5. M. Kerker, *The scattering of light and other electromagnetic radiation: physical chemistry: a series of monographs*, vol. 16 (Academic press, 2013).
6. J. D. Jackson, *Classical Electrodynamics* (Wiley, 1999).
7. T. Wriedt, "Mie theory: a review," in *The Mie Theory* (Springer, 2012), pp. 53–71.
8. A. Zangwill, *Modern Electrodynamics* (Cambridge University, 2013).
9. A. Moroz, "A recursive transfer-matrix solution for a dipole radiating inside and outside a stratified sphere," Ann. Phys. **315**(2), 352–418 (2005).
10. R. Dezert, P. Richetti, and A. Baron, "Isotropic Huygens dipoles and multipoles with colloidal particles," Phys. Rev. B **96**(18), 180201 (2017).
11. V. Cachorro and L. Salcedo, "New improvements for Mie scattering calculations," J. Electromagn. Waves Appl. **5**(9), 913–926 (1991).
12. D. Tzarouchis and A. Sihvola, "Light scattering by a dielectric sphere: perspectives on the Mie resonances," Appl. Sci. **8**(2), 184 (2018).
13. M. Alam and Y. Massoud, "A closed-form analytical model for single nanoshells," IEEE Trans. Nanotechnol. **5**(3), 265–272 (2006).
14. J. Shen, "Algorithm of numerical calculation on lorentz Mie theory," PIERS Online **1**(6), 691–694 (2005).
15. H. C. Hulst and H. C. van de Hulst, *Light scattering by small particles* (Courier Corporation, 1981).
16. J. A. Adam, "Scattering of electromagnetic plane waves in radially inhomogeneous media: ray theory, exact solutions and connections with potential scattering theory," in *Light Scattering Reviews 9* (Springer, 2015) pp. 101–132.
17. W. T. Grandy Jr and W. T. Grandy, *Scattering of waves from large spheres* (Cambridge University, 2005).
18. R. G. Newton, *Scattering theory of waves and particles* (Springer Science & Business Media, 2013).
19. R. Gómez-Medina, P. San José, A. García-Martín, M. Lester, M. Nieto-Vesperinas, and J. Sáenz, "Resonant radiation pressure on neutral particles in a waveguide," Phys. Rev. Lett. **86**(19), 4275–4277 (2001).
20. A. García-Etxarri, R. Gómez-Medina, L. S. Froufe-Pérez, C. López, L. Chantada, F. Scheffold, J. Aizpurua, M. Nieto-Vesperinas, and J. J. Sáenz, "Strong magnetic response of submicron silicon particles in the infrared," Opt. Express **19**(6), 4815–4826 (2011).
21. A. Rahimzadegan, R. Alaee, I. Fernandez-Corbaton, and C. Rockstuhl, "Fundamental limits of optical force and torque," Phys. Rev. B **95**(3), 035106 (2017).
22. A. Rahimzadegan, D. Arslan, D. Dams, A. Groner, X. Garcia-Santiago, R. Alaee, I. Fernandez-Corbaton, T. Pertsch, I. Staude, and C. Rockstuhl, "Beyond dipolar Huygens' metasurfaces for full-phase coverage and unity transmittance," Nanophotonics **9**(1), 75–82 (2019).
23. J. Olmos-Trigo, D. R. Abujetas, C. Sanz-Fernández, J. A. Sánchez-Gil, and J. J. Sáenz, "Optimal backward light scattering by dipolar particles," Phys. Rev. Res. **2**(1), 013225 (2020).
24. N. Engheta and R. W. Ziolkowski, *Metamaterials: physics and engineering explorations* (John Wiley & Sons, 2006).
25. F. Capolino, *Theory and phenomena of metamaterials* (CRC press, 2017).
26. I. Staude and J. Schilling, "Metamaterial-inspired silicon nanophotonics," Nat. Photonics **11**(5), 274–284 (2017).
27. Q. Zhao, J. Zhou, F. Zhang, and D. Lippens, "Mie resonance-based dielectric metamaterials," Mater. Today **12**(12), 60–69 (2009).
28. H.-T. Chen, A. J. Taylor, and N. Yu, "A review of metasurfaces: physics and applications," Rep. Prog. Phys. **79**(7), 076401 (2016).
29. P. Lalanne and P. Chavel, "Metalenses at visible wavelengths: past, present, perspectives," Laser Photonics Rev. **11**(3), 1600295 (2017).
30. E. Karimi, S. A. Schulz, I. De Leon, H. Qassim, J. Upham, and R. W. Boyd, "Generating optical orbital angular momentum at visible wavelengths using a plasmonic metasurface," Light: Sci. Appl. **3**(5), e167 (2014).
31. H. K. Shamkhi, K. V. Baryshnikova, A. Sayanskiy, P. Kapitanova, P. D. Terekhov, P. Belov, A. Karabchevsky, A. B. Evlyukhin, Y. Kivshar, and A. S. Shalin, "Transverse scattering and generalized kerker effects in all-dielectric Mie-resonant metaoptics," Phys. Rev. Lett. **122**(19), 193905 (2019).
32. O. Quevedo-Teruel, H. Chen, A. Díaz-Rubio, G. Gok, A. Grbic, G. Minatti, E. Martini, S. Maci, G. V. Eleftheriades, M. Chen, N. I. Zheludev, N. Papasimakis, S. Choudhury, Z. A. Kudyshev, S. Saha, H. Reddy, A. Boltasseva, V. M. Shalaev, A. V. Kildishev, D. Sievenpiper, C. Caloz, A. Alú, Q. He, L. Zhou, G. Valerio, E. Rajo-Iglesias, Z. Sipus, F. Mesa, R. Rodriguez-Berral, F. Medina, V. Asadchy, S. Tretyakov, and C. Craeye, "Roadmap on metasurfaces," J. Opt. **21**(7), 073002 (2019).

Optics EXPRESS

33. J. Proust, F. Bedu, B. Gallas, I. Ozerov, and N. Bonod, "All-dielectric colored metasurfaces with silicon Mie resonators," ACS Nano **10**(8), 7761–7767 (2016).
34. A. Krasnok, S. Makarov, M. Petrov, R. Savelev, P. Belov, and Y. Kivshar, "Towards all-dielectric metamaterials and nanophotonics," in *Metamaterials X*, vol. 9502 (International Society for Optics and Photonics, 2015), p. 950203.
35. M. Rahmani, L. Xu, A. E. Miroshnichenko, A. Komar, R. Camacho-Morales, H. Chen, Y. Zárate, S. Kruk, G. Zhang, D. N. Neshev, and Y. S. Kivshar, "Reversible thermal tuning of all-dielectric metasurfaces," Adv. Funct. Mater. **27**(31), 1700580 (2017).
36. M. M. Hossain and M. Gu, "Radiative cooling: Principles, progress, and potentials," Adv. Sci. **3**(7), 1500360 (2016).
37. X. Zhang, H. Liu, Z. Zhang, Q. Wang, and S. Zhu, "Controlling thermal emission of phonon by magnetic metasurfaces," Sci. Rep. **7**(1), 41858 (2017).
38. A. Ghanekar, L. Lin, and Y. Zheng, "Novel and efficient Mie-metamaterial thermal emitter for thermophotovoltaic systems," Opt. Express **24**(10), A868–A877 (2016).
39. L. Huang, X. Chen, H. Mühlenbernd, H. Zhang, S. Chen, B. Bai, Q. Tan, G. Jin, K.-W. Cheah, C.-W. Qiu, J. Li, T. Zentgraf, and S. Zhang, "Three-dimensional optical holography using a plasmonic metasurface," Nat. Commun. **4**(1), 2808 (2013).
40. R. Alaee, M. Albooyeh, and C. Rockstuhl, "Theory of metasurface based perfect absorbers," J. Phys. D: Appl. Phys. **50**(50), 503002 (2017).
41. Y. Ra'Di, C. Simovski, and S. Tretyakov, "Thin perfect absorbers for electromagnetic waves: theory, design, and realizations," Phys. Rev. Appl. **3**(3), 037001 (2015).
42. A. B. Evlyukhin, K. V. Nerkararyan, and S. I. Bozhevolnyi, "Core-shell particles as efficient broadband absorbers in infrared optical range," Opt. Express **27**(13), 17474–17481 (2019).
43. R. Dezert, P. Richetti, and A. Baron, "Complete multipolar description of reflection and transmission across a metasurface for perfect absorption of light," Opt. Express **27**(19), 26317–26330 (2019).
44. T. Geng, S. Zhuang, J. Gao, and X. Yang, "Nonlocal effective medium approximation for metallic nanorod metamaterials," Phys. Rev. B **91**(24), 245128 (2015).
45. M. Silveirinha, J. Baena, L. Jelinek, and R. Marques, "Nonlocal homogenization of an array of cubic particles made of resonant rings," Metamaterials **3**(3-4), 115–128 (2009).
46. P. Genevet and F. Capasso, "Holographic optical metasurfaces: a review of current progress," Rep. Prog. Phys. **78**(2), 024401 (2015).
47. X. Ni, A. V. Kildishev, and V. M. Shalaev, "Metasurface holograms for visible light," Nat. Commun. **4**(1), 2807 (2013).
48. G. Zheng, H. Mühlenbernd, M. Kenney, G. Li, T. Zentgraf, and S. Zhang, "Metasurface holograms reaching 80% efficiency," Nat. Nanotechnol. **10**(4), 308–312 (2015).
49. S. M. Kamali, E. Arbabi, A. Arbabi, and A. Faraon, "A review of dielectric optical metasurfaces for wavefront control," Nanophotonics **7**(6), 1041–1068 (2018).
50. M. Albooyeh, S. Kruk, C. Menzel, C. Helgert, M. Kroll, A. Krysinski, M. Decker, D. N. Neshev, T. Pertsch, C. Etrich, and R. Carsten, "Resonant metasurfaces at oblique incidence: interplay of order and disorder," Sci. Rep. **4**(1), 4484 (2015).
51. A. Rahimzadegan, D. Arslan, R. Suryadharma, S. Fasold, M. Falkner, T. Pertsch, I. Staude, and C. Rockstuhl, "Disorder-induced phase transitions in the transmission of dielectric metasurfaces," Phys. Rev. Lett. **122**(1), 015702 (2019).
52. A. Jouanin, J. P. Hugonin, and P. Lalanne, "Designer colloidal layers of disordered plasmonic nanoparticles for light extraction," Adv. Funct. Mater. **26**(34), 6215–6223 (2016).
53. D. G. Grier, "A revolution in optical manipulation.," Nature **424**(6950), 810–816 (2003).
54. M. Dienerowitz, M. Mazilu, and K. Dholakia, "Optical manipulation of nanoparticles: a review," J. Nanophotonics **2**(1), 021875 (2008).
55. C. Guclu, V. A. Tamma, H. K. Wickramasinghe, and F. Capolino, "Photoinduced magnetic force between nanostructures," Phys. Rev. B **92**(23), 235111 (2015).
56. M. Nieto-Vesperinas, R. Gomez-Medina, and J. Saenz, "Angle-suppressed scattering and optical forces on submicrometer dielectric particles," J. Opt. Soc. Am. A **28**(1), 54–60 (2011).
57. M. Nieto-Vesperinas, J. Sáenz, R. Gómez-Medina, and L. Chantada, "Optical forces on small magnetodielectric particles," Opt. Express **18**(11), 11428–11443 (2010).
58. Z. Ruan and S. Fan, "Design of subwavelength superscattering nanospheres," Appl. Phys. Lett. **98**(4), 043101 (2011).
59. X. Zambrana-Puyalto, X. Vidal, M. L. Juan, and G. Molina-Terriza, "Dual and anti-dual modes in dielectric spheres," Opt. Express **21**(15), 17520–17530 (2013).
60. C. F. Bohren, "Recurrence relations for the Mie scattering coefficients," J. Opt. Soc. Am. A **4**(3), 612–613 (1987).
61. P. Lambropoulos and D. Petrosyan, *Fundamentals of quantum optics and quantum information*, vol. 23 (Springer, 2007).
62. S. Tretyakov, "Maximizing absorption and scattering by dipole particles," Plasmonics **9**(4), 935–944 (2014).
63. M. I. Abdelrahman, C. Rockstuhl, and I. Fernandez-Corbaton, "Broadband suppression of backscattering at optical frequencies using low permittivity dielectric spheres," Sci. Rep. **7**(1), 14762 (2017).
64. B. Hopkins, W. Liu, A. E. Miroshnichenko, and Y. S. Kivshar, "Optically isotropic responses induced by discrete rotational symmetry of nanoparticle clusters," Nanoscale **5**(14), 6395–6403 (2013).

Optics EXPRESS

65. D. W. Mackowski, "Calculation of total cross sections of multiple-sphere clusters," J. Opt. Soc. Am. A **11**(11), 2851–2861 (1994).
66. D. W. Mackowski and M. I. Mishchenko, "Calculation of the t matrix and the scattering matrix for ensembles of spheres," J. Opt. Soc. Am. A **13**(11), 2266–2278 (1996).
67. Y. Xu, "Electromagnetic scattering by an aggregate of spheres.," Appl. Opt. **34**(21), 4573–4588 (1995).
68. R. Alaee, C. Rockstuhl, and I. Fernandez-Corbaton, "Exact multipolar decompositions with applications in nanophotonics," Adv. Opt. Mater. **7**(1), 1800783 (2019).
69. A. Rahimzadegan, C. Rockstuhl, and I. Fernandez-Corbaton, "Core-shell particles as building blocks for systems with high duality symmetry," Phys. Rev. Appl. **9**(5), 054051 (2018).
70. M. Z. Alam, I. De Leon, and R. W. Boyd, "Large optical nonlinearity of indium tin oxide in its epsilon-near-zero region," Science **352**(6287), 795–797 (2016).
71. J. Peurifoy, Y. Shen, L. Jing, Y. Yang, F. Cano-Renteria, B. G. DeLacy, J. D. Joannopoulos, M. Tegmark, and M. Soljačić, "Nanophotonic particle simulation and inverse design using artificial neural networks," Sci. Adv. **4**(6), eaar4206 (2018).
72. I. Fernandez-Corbaton and C. Rockstuhl, "Unified theory to describe and engineer conservation laws in light-matter interactions," Phys. Rev. A **95**(5), 053829 (2017).